BULLETIN OF THE POLISH ACADEMY OF SCIENCES
TECHNICAL SCIENCES
DOI:10.24425 10.24425/bpasts.2025.153435

Bending behaviour of thin-walled perforated channel beams with modified cross sectional shape – Part 2: analytical calculations and FEM

Paweł Jasion[1], Aleksandra M. Pawlak[1*], Piotr Paczos[1], Michał Plust[1] and Marcin Rodak[1]

[1] Poznań University of Technology, Institute of Applied Mechanics, Jana Pawła II 24, 60-965 Poznań, Poland

Abstract. This article is the second part of a comprehensive research program investigating the structural performance of thin-walled channels with modified cross-sectional geometries. The study involved testing six beams, three of which featured perforated webs, while the other three had flat, solid webs. The beams were subjected to four-point bending tests to evaluate their load-bearing capacity. The first part of the research presented the results of experimental tests and finite strip analysis. This article will focus on finite element analyses and analytical calculations conducted in accordance with Eurocode 3 guidelines and the principle of minimizing potential energy. The study provides several significant contributions: it integrates experimental, numerical, and theoretical methods to deliver a thorough evaluation of beam performance. The finite element method (FEM) simulations offer precise modeling of complex stress and strain states, while analytical calculations supply a solid theoretical foundation for interpreting structural behavior. The research demonstrates that web perforation, while reducing critical and maximum forces, also results in considerable weight savings, enhancing material efficiency. Additionally, the division of the research into two articles ensures clarity and accessibility, with this second part dedicated to detailed FEM and analytical results, thereby facilitating both academic understanding and practical engineering applications.

Key words: thin-walled channel beams; web perforations; four-point bending; structural stability; buckling analysis

1. INTRODUCTION

Thin-walled structures produced through cold-forming technology are widely utilized across various fields, including civil engineering, the transportation sector (such as automotive and railway applications), and the aerospace industry. In contemporary engineering practice, there is a growing emphasis on minimizing material usage while maintaining structural integrity. Thin-walled structures address this objective effectively due to their high strength-to-weight ratio and low material consumption. Additionally, these structures are advantageous in terms of ease of assembly, further contributing to their appeal in both industrial and structural applications.

Thin-walled structures with modified or non-standard cross sections are increasingly studied for their structural stability and buckling behavior, particularly when incorporating web perforations. Research indicates that these modifications can significantly influence the load-bearing capacity and overall stability of the structures. For instance, incorporating perforations into web sections can result in a reduction of mass while preserving structural integrity. However, such modifications may also render the structure more prone to buckling under specific conditions, as can be found in the studies by Roslanec and Rozylo [1] and Bakhach et al. [2] .In addition, the effectiveness of different cross-sectional shapes in enhancing stability has been investigated, revealing that custom geometries can outperform traditional designs in certain applications, as can be read in the work of Rozylo et al. [3], [4]. However, the performance of these modified structures is highly dependent on the configuration and size of the perforations, which necessitates careful design considerations to mitigate potential buckling risks. Overall, while innovative cross-sectional designs present opportunities for improved performance, they also require thorough analysis to ensure safety and reliability in engineering applications.

Heavily modified cross-sectional shapes have been thoroughly described in the works of Grenda and Paczos [5], Grenda [6], Pawlak and Paczos [7], and Jasion et al. [8], Obst et al. [9], Magnucka-Blandzi et al. [10] where beams/columns subjected to four-point bending or axial compression were analyzed. Nevertheless, most researchers continue to focus on traditional cross-sectional shapes, failing to recognize that these modifications can positively impact the stability of thin-walled structures and increase their critical strength [11], [12], [13]. The use of modified cross-sections in thin-walled

*e-mail: aleksandra.pawlak@put.poznan.pl

structures offers numerous advantages, such as enhanced bending strength and improved stability, leading to greater load-bearing capacity and extended service life of the structure. These modifications allow for significant weight reduction while maintaining or even improving strength, resulting in material savings and reduced costs. Additionally, altered cross-sectional shapes can streamline production and assembly processes, as well as enhance the aesthetics and functionality of structures, enabling better adaptation to specific loading and environmental conditions.

Numerical investigations are crucial for analyzing thin-walled structures, with the finite element method (FEM) being one of the most frequently employed techniques. Numerical studies can be conducted using various methods, with FEM being one of the most prevalent, as applied in this paper. Anbarasu [14] utilized FEM to investigate the local, distortional, and flexural-torsional buckling behavior of cold-formed steel (CFS) beams. Dinis and Camotim [15] explored the post-buckling behavior of channel columns subjected to bending moments, focusing on the interaction between local and strain buckling using FEM. El Hadidy et al. [16] examined beams with trapezoidal webs through FEM. Ghorashi [17] employed the Variational Asymptotic Method to address problems related to thin-walled structures, applying it for nonlinear static analysis and stability analysis of composite beams. Both finite difference and finite element methods were utilized to calculate the elastic deformations of beams with clamped-free boundary conditions. The paper [18] presents a numerical analysis of magnetohydrodynamic mixed convection heat transfer in a lid-driven wavy enclosure with a fin attached to the bottom wall, utilizing the finite element method. Results demonstrate that fin size plays a crucial role in influencing flow patterns and temperature distribution, with larger fins significantly enhancing heat transfer at higher Richardson numbers and lower Hartmann numbers. In the article [19], damage detection in an aluminum beam using vibration techniques showed that increasing crack depth raised amplitude. Experimental validation confirmed the method's accuracy, with errors of 7.5% for crack position and 9.1% for crack size.

The work of Manikandan and Thulasi [20] investigated the behavior of cold-formed I-section steel plates with edge and intermediate web stiffening under bending loads. Their research involved optimizing the cross-section using numerical methods (FEM), followed by experimental tests employing strain gauges, and concluded with calculations based on Eurocode 3 procedures. Nandini and Kalyanaraman [21] conducted a study using ABAQUS for finite element analysis, examining the interaction between local, strain, and bending-torsion buckling forms. Kubiak and Gliszczynski [22] assessed the load capacity of thin-walled composite channel beams subjected to pure bending using ANSYS software and FEM. Zhang and Young [23] developed a finite element model to account for initial geometric imperfections and nonlinear material properties, applying it to analyze cold-formed thin-walled structures with web stiffening. Falkowicz and Debski [24] analyzed thin-walled plate elements with regular-shaped cutouts, employing both digital image correlation and FEM in their study. Debski [25] investigated the effect of eccentric loading on the stability and post-critical states of thin-walled composite columns in compression, designing and verifying numerical models of thin-walled composite sections based on FEM analysis.

The motivation for this study stems from a notable gap in the existing literature concerning the analysis of thin-walled sections with modified cross-sectional geometries. This research seeks to address this gap by examining the effects of web perforations on both critical and maximum forces, thereby offering valuable insights into the trade-offs between weight reduction and structural performance. The findings of this investigation are expected to inform more refined design practices and enhance the safety and effectiveness of thin-walled structural members across various engineering applications.

2. GEOMETRY OF CROSS SECTIONS

In this chapter, a brief overview of the subject of study is presented, as it has already been comprehensively described in Part 1 of this article, titled *"Bending Behaviour of Thin-Walled Perforated Channel Beams with Modified Cross Sectional Shape – Part 1: Experimental Tests and FSM."* This study focuses on six thin-walled, cold-formed channel beams (B1–B6) with modified cross-sectional configurations, where three beams have solid webs (B1, B3, and B5), and three have perforated webs (B2, B4, and B6). The dimensions of the beam cross sections are shown in Figure 1 and Table 1.

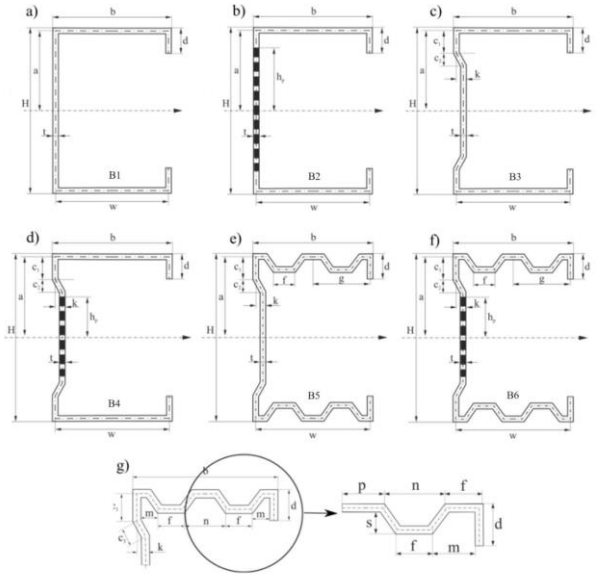

Fig.1. Dimensioned cross-sections of the analyzed beams

TABLE 1. Dimensions of the cross-sections of the beams

H	=	*160.0*	*mm*
b	=	80.0	mm
a	=	79.5	mm
w	=	79.0	mm
d	=	18.0	mm
h_{p2}	=	68.5	mm
$h_{p4,6}$	=	40.0	mm
k	=	8.0	mm

c_1	=	*18.0*	*mm*
c_2	=	10.0	mm
c_3	=	10.0	mm
f	=	10.0	mm
g	=	36.0	mm
n	=	24.0	mm
m	=	18.0	mm
s	=	15.0	mm

Figure 2 illustrates the dimensions of the perforations and provides an image of the perforated beam web.

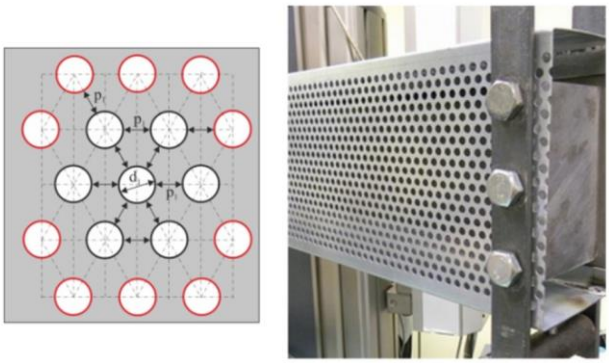

Fig.2. Geometry and dimension of perforations

In Part 1, the mechanical properties of the steel used to manufacture the beams were described in detail. These properties were determined based on results obtained from a static tensile test.

3. ANALYTICAL CALCULATIONS

Analytical calculations were conducted to determine the critical moments of the beams subjected to bending, focusing on beams B1, B3, and B5. Beams B2, B4, and B6, which feature perforations in the web, were excluded from these analyses due to Eurocode 3's limitation in accommodating significant modifications in cross-sectional shapes. The challenge of developing formulas for critical moments in these complex geometries further complicated their inclusion, as Eurocode 3 only addresses single additional bends. This chapter presents the mathematical formulas implemented in MATLAB for efficient and accurate calculations, along with the resulting data.

The mathematical formulas presented in this chapter have been developed based on the principle of minimum total potential energy [26], [27], [28]. This principle serves as a fundamental basis in the analysis of rigid body mechanics, allowing for the determination of equilibrium and stability conditions in structures. By utilizing this method, it is possible to accurately model the behaviors of beams, which is crucial for understanding their responses to various loads. Basing the calculations on this principle also enables more precise results and effective predictions of structural behaviors under real-world conditions.

This study presents comprehensive analytical calculations for global, local, and distortional buckling. However, it is evident that thin-walled structures do not experience global buckling. The mathematical formulas introduced in this work have been implemented into MATLAB, where a specialized program was developed to calculate critical forces for beams with arbitrary cross-sectional sizes and lengths. Additionally, this work aims to demonstrate how the prepared program computes these critical force values.

3.1. Calculation procedure - theoretical introduction to analytical calculations

Pure bending is simulated by a four-point bending test. The total length of the beam is denoted by L_c, the distance between the applied force and the supports equals L_s and the distance between supports is equal to L_0. The part of the beam which is under pure bending conditions has the length L. Thus, the critical moment M_{cr} in the middle span of the beam can be calculated using the following formula:

$$M_{cr} = \frac{1}{2} F_{cr} L_s = \frac{1}{4} F_{cr} L_s \tag{1}$$

where F_{cr} is critical force. Thin-walled beams are susceptible to loss of stability because of the high ratio of length and cross-sectional dimensions to plate thickness. In the context of thin-walled structures, we distinguish three types of loss of stability: general buckling, local buckling and distortional buckling. This paper presents a procedure for determining the values of critical moments for the different forms of buckling of thin-walled beams.

The critical state of a thin-walled beam that was loaded with a bending moment of constant value was determined using energy methods. The energy or elastic deformation U_ε can be defined as follows:

$$U_\varepsilon = U_{\varepsilon l} + U_{\varepsilon n} \tag{2}$$

where $U_{\varepsilon l}$ is linear elastic deformation energy and $U_{\varepsilon n}$ is nonlinear elastic deformation energy. Components of energy are expressed in the following form:

$$\begin{aligned} U_{\varepsilon l} = \frac{1}{2} E \int_0^L \Bigg[& A \left(\frac{\mathrm{d}u}{\mathrm{d}x}\right)^2 + J_z \left(\frac{\mathrm{d}^2 v}{\mathrm{d}x^2}\right)^2 + 2 J_{yz} \frac{\mathrm{d}^2 v}{\mathrm{d}x^2} \frac{\mathrm{d}^2 w}{\mathrm{d}x^2} \\ & + J_y \left(\frac{\mathrm{d}^2 w}{\mathrm{d}x^2}\right)^2 + J_\omega \left(\frac{\mathrm{d}^2 \psi}{\mathrm{d}x^2}\right)^2 \Bigg] \mathrm{d}x \\ & + \frac{1}{2} G \int_0^L J_t \left(\frac{\mathrm{d}\psi}{\mathrm{d}x}\right)^2 \mathrm{d}x \\ & + \frac{1}{2} \int_0^L \left[k_y v_P^2 + k_z w_P^2 + k_\psi \psi^2 \right] \mathrm{d}x \end{aligned} \tag{3}$$

$$U_{\varepsilon n} = \frac{1}{2}\int_0^L N\left[\left(\frac{\mathrm{d}v}{\mathrm{d}x}\right)^2 + \left(\frac{\mathrm{d}w}{\mathrm{d}x}\right)^2\right]\mathrm{d}x + \frac{1}{2}\int_0^L \left[r_S^2 N + 2\beta_{Sz}M_y - 2\beta_{Sy}M_z + 2\beta_\omega B\right]\left(\frac{\mathrm{d}\psi}{\mathrm{d}x}\right)^2 \mathrm{d}x + \int_0^L \left[M_y\frac{\mathrm{d}^2 v}{\mathrm{d}x^2} + M_z\frac{\mathrm{d}^2 w}{\mathrm{d}x^2}\right]\psi\mathrm{d}x + \int_0^L N\left[z_S\frac{\mathrm{d}v}{\mathrm{d}x} - y_S\frac{\mathrm{d}w}{\mathrm{d}x}\right]\frac{\mathrm{d}\psi}{\mathrm{d}x}\mathrm{d}x \quad (4)$$

where G is Kirchhoff's modulus, E is Young's modulus and A is a cross sectional area of the beam. The next designations are: u, v, w – shear center displacement S; J_z, J_{yz}, J_y – moment of inertia of the beam; J_ω – wrapping moment, J_t – the Saint-Venant torsion constant; k_y, k_z, k_ψ – spring rates in the flange model for distortional buckling; $\beta_{sz}, \beta_{sy}, \beta_\omega$ – Wagner's coefficient; u_P, v_P, w_P – displacement components of the point P, r_s^2 – polar radius of the inertia about the shear center S, ψ – torsion angle, N – axial force, M_y, M_z – bending moment about y and z axis, B – bimoment, z_s, y_s – coordinates of the shear center S.

3.1.1. Global buckling

Dislocation of thin-walled beams is characterized by simultaneous torsion of the beam and its spatial bending. The analysis assumes that the cross section of the beam does not change its shape. Figure 3 shows a general stability diagram for a beam with a non-standard cross-section shape.

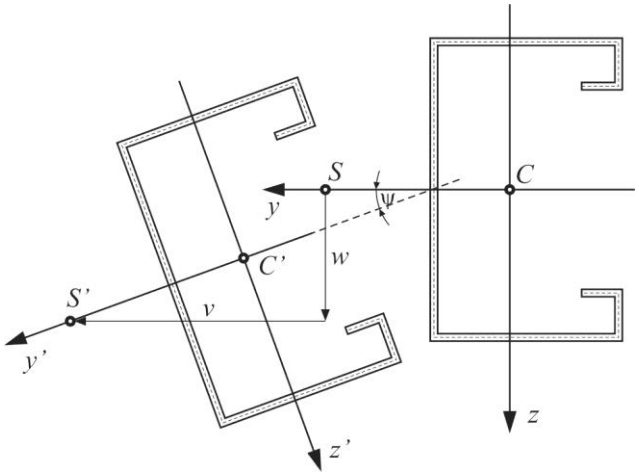

Fig. 3. Schematic of general loss of stability for a thin-walled beam with modified cross-sectional shape

As the buckling half-wave length increases, the value of the critical force or moment decreases. The angle of rotation for general buckling for beams simply supported at both ends for any coordinate x can be represented by a mathematical formula:

$$\frac{v}{v_1} = \frac{u}{u_1} = \frac{\psi(x)}{\psi_1} = \sin\frac{\pi x}{L} \quad (5)$$

where ψ_1 is a dimensionless parameter. The bending moment can be written as:

$$M_y(x) = M_0 \quad (6)$$

The derived system of second order equilibrium equations was used to determine the critical moment for general buckling:

$$N, M_z, B = 0;\ \ I_{yz}, \beta_{Sz}, \beta_\omega = 0 \quad (7)$$

$$k_y, k_z, k_\psi = 0 \quad (8)$$

Thus, based on Eq. (3) and Eq. (4) an expression describing the elastic strain energy of the form was obtained:

$$U_\varepsilon = \frac{1}{2}\int_0^L \left[EJ_z\left(\frac{d^2 v}{dx^2}\right)^2 + EJ_y\left(\frac{d^2 w}{dx^2}\right)^2 + EJ_\omega\left(\frac{d^2\psi}{dx^2}\right)^2 + GJ_t\left(\frac{d\psi}{dx}\right)^2\right]dx + \int_0^L M_y\frac{d^2 v}{dx^2}\psi dx \quad (9)$$

The work of external forces W is written using the following formula:

$$W = -M_y\frac{\mathrm{d}w}{\mathrm{d}x}\Big|_0^L \quad (10)$$

It is defined that $w(x)$ is the displacement in the z-axis direction and $v(x)$ is the displacement in the y-axis direction. The formula describing the critical moment at general buckling was determined:

$$M_{cr}^{(global)} = \frac{\pi}{L}\sqrt{EJ_z\left[GJ_t + \left(\frac{\pi}{L}\right)^2 EJ_\omega\right]} \quad (11)$$

The above transformations led to a formula that will be used to determine the critical moment for global buckling.

3.1.2. Distortional buckling

Considering the loss of beam stability by buckling of the flange with simultaneous deformation of the web, the flange can be treated as an elastically supported beam at the edge of its connection with the web (point $P(y_p, z_p)$ of the cross-

section). Figure 4 shows the buckling model and the cross-section of the beam and flange. A central coordinate system $(x, \bar{y}, \bar{z})$, centred at $\overline{C}$, is associated with the shelf.

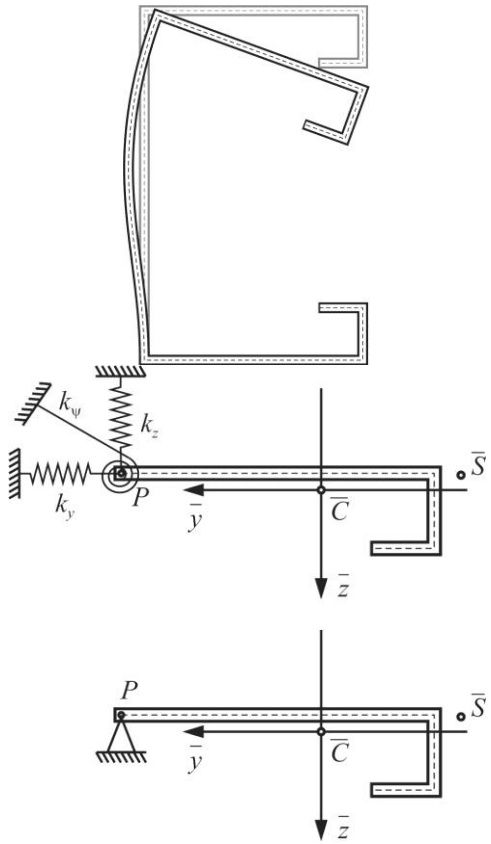

Fig. 4. Distortional stability loss diagram of a beam with a modified cross-section

There are normal stresses in the flange, which can be expressed by the following mathematical formula:

$$\sigma_x(x, \bar{y}, \bar{z}) = \frac{M_y}{J_y}(\bar{z} - \bar{z}_C) \tag{12}$$

Where $(\bar{y}, \bar{z})$ is the central coordinate system associated with the beam flange, and $\bar{z}_C$ is the coordinate of the beam section center in the coordinate system associated with the flange. It can be seen that there is a relationship with $\bar{z}_C = -z_{\bar{c}}$. The internal forces present in the flange can be expressed by the formula:

$$\bar{N} = -\frac{M_y}{J_y}\bar{z}_C\bar{A}, \quad \bar{M}_{\bar{y}} = \frac{M_y}{J_y}\bar{J}_{\bar{y}}, \quad \bar{M}_{\bar{z}} = -\frac{M_y}{J_y}\bar{J}_{\bar{y}\bar{z}}, \quad \bar{B} = 0 \tag{13}$$

The model was simplified, as shown in figure 5. After simplifying $\bar{v}_P = 0$, $\bar{w}_P = 0$ and $k_\psi = 0$ we get:

$$\bar{v} = (\bar{z}_P - \bar{z}_{\bar{S}})\bar{\psi} \tag{14}$$

$$\bar{w} = -(\bar{y}_P - \bar{y}_{\bar{S}})\bar{\psi} \tag{15}$$

The strain energy of the beam flange equals:

$$\begin{aligned} U_\varepsilon^{(flange)} = {} & \frac{1}{2}E\bar{J}_{\bar{\omega}_P}\int_0^L\left(\frac{\mathrm{d}^2\bar{\psi}}{\mathrm{d}x^2}\right)^2\mathrm{d}x \\ & + \frac{1}{2}G\bar{J}_t\int_0^L\left(\frac{\mathrm{d}\bar{\psi}}{\mathrm{d}x}\right)^2\mathrm{d}x \\ & - \frac{1}{2}\frac{M_y}{I_y}\left[\bar{r}_P^2\bar{z}_C\bar{A} - 2\bar{\beta}_{P\bar{z}}\bar{J}_{\bar{y}}\right. \\ & \left. - 2\bar{\beta}_{P\bar{y}}\bar{J}_{\bar{y}\bar{z}}\right]\int_0^L\left(\frac{\mathrm{d}\bar{\psi}}{\mathrm{d}x}\right)^2\mathrm{d}x \end{aligned} \tag{16}$$

where:

$$\begin{aligned} \bar{r}_P^2 &= \frac{\bar{J}_{\bar{y}} + \bar{J}_{\bar{z}}}{\bar{A}} + \bar{y}_P^2 + \bar{z}_P^2 \\ \bar{J}_{\bar{\omega}_P} &= \bar{J}_{\bar{\omega}} + (\bar{y}_P - \bar{y}_{\bar{S}})^2\bar{J}_{\bar{y}} - 2(\bar{y}_P - \bar{y}_{\bar{S}})(\bar{z}_P - \bar{z}_{\bar{S}})\bar{J}_{\bar{y}\bar{z}} + (\bar{z}_P - \bar{z}_{\bar{S}})^2\bar{J}_{\bar{z}} \\ \bar{\beta}_{P\bar{y}} &= \bar{\beta}_{\bar{S}\bar{y}} + \bar{y}_{\bar{S}} - \bar{y}_P, \qquad \bar{\beta}_{P\bar{z}} = \bar{\beta}_{\bar{S}\bar{z}} + \bar{z}_{\bar{S}} - \bar{z}_P \end{aligned} \tag{17}$$

The critical moment was calculated from the equation:

$$\delta(U_\varepsilon) = 0 \tag{18}$$

By substituting the expression:

$$\bar{\psi}(x) = \psi_1 \sin\frac{\pi x}{L} \tag{19}$$

and solving the equation using the Ritz method, we obtain the formula describing the critical moment for distortional buckling:

$$M_{cr}^{(distortional)} = \frac{G\bar{J}_t + E\bar{J}_{\bar{\omega}_P}\left(\frac{\pi}{L}\right)^2}{\bar{r}_P^2\bar{z}_C\bar{A} - 2\bar{\beta}_{P\bar{y}}\bar{J}_{\bar{y}} - 2\bar{\beta}_{P\bar{z}}J_{\bar{y}\bar{z}}}J_y \tag{20}$$

The above transformations led to the formula that will be used to determine the critical moment for distortional buckling.

3.1.3. Local buckling

Local stability is characterized by the fact that the length of the buckling half-wave is comparable to the transverse dimensions of the beam and is most often considered as buckling of individual beam walls. In this paper, local buckling is considered as buckling of individual beam walls:

- hinged at the four edges - spanning walls (figure 5a),
- hinged on three edges and one free edge - cantilever walls (figure 5b).

The critical state of a thin-walled beam that was loaded with a bending moment of constant value was determined using energy methods.

Figure 5 shows the beam support scheme in the local coordinate system (x, η, ς) associated with the beam wall. Rectangular walls are shown.

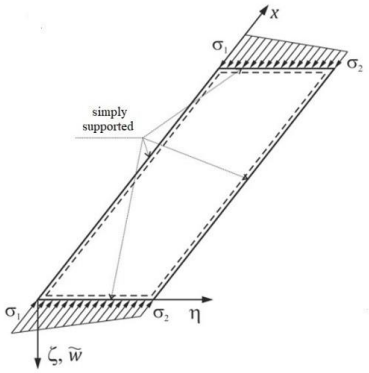

(a) span structure

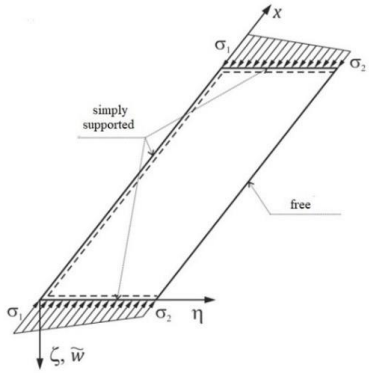

(b) cantilevered structure

Fig. 5. Beam support scheme

The procedures for determining the critical moment for local buckling are well known, as they are described in detail in PN-EN 1993-1-5 [29]. The standard distinguishes between two ways of supporting a wall: spanning compression walls and cantilever compression walls. A simplified model is adopted in which the critical stress is calculated from the formula:

$$\sigma_{cr} = \frac{M_{cr}}{J_y} y_R \tag{21}$$

From Eq. (21), the value of the critical moment can be determined:

$$M_{cr} = \frac{J_y}{y_R} \sigma_{cr} \tag{22}$$

The critical stress for pure bending and the corresponding factor κ are calculated. Let's denote $\sigma_1 = \max(-\sigma_x) > 0$ and $\sigma_1 = \kappa \frac{\pi^2 D}{tb^2} = \kappa \frac{\pi^2 E}{12(1-\nu^2)} \left(\frac{t}{b}\right)^2$, Therefore, for a spanning wall, the stresses can be expressed by the formula:

$$\begin{aligned} \sigma_x(x, \eta) &= -\left(1 - \frac{\eta}{b}\right)\sigma_1 - \frac{\eta}{b}\sigma_2 \\ &= -\sigma_1 \left[\left(1 - \frac{\eta}{b}\right) + \frac{\eta}{b}\psi\right] \end{aligned} \tag{23}$$

where $\psi = \frac{\sigma_2}{\sigma_1}$, σ_2 - see figure 5, b is the beam width and t is the thickness of the plate from which the beams were made. Critical values for the coefficient κ were obtained, e.g. for $\psi = 1$ $\kappa = 4$ and for $\psi = -1$ κ is about 24. These values are valid for sufficiently long beams. For a cantilevered, pinned wall supported on three edges and one free edge, $\eta = 0$. However, for a spanning, pinned wall supported on four edges, $\eta = b$. This data was obtained on the basis of the indicated standard. In summary, the critical moment value for local buckling is expressed by the formula:

$$\begin{aligned} M_{y,cr}^{(local)} = \frac{J_y}{y_R}\left(\frac{6}{\pi^2}(1-\nu) + \frac{1}{\lambda^2}\right) \times \frac{4}{1+3\psi} \\ \times \frac{\pi^2 E}{12(1-\nu^2)}\left(\frac{t}{b}\right)^2 \end{aligned} \tag{24}$$

where $R\ (y_R, z_R)$ is the point lying at one end of the wall centreline. At the point where the compressive stresses reach their maximum stresses are denoted σ_1, while at the other end σ_2.

3.2. Results of calculations

The results of the analytical calculations presented in this chapter were obtained using a specialized program that applies the analytical formulas outlined herein. This program, named GUI, was developed in MATLAB and authored by Dr. Marcin Rodak. The first step in the process involves specifying the beam lengths, the span between supports, and identifying the mechanical properties. For the purposes of this article, the mechanical properties implemented in the program were determined through static tensile tests, as detailed in Chapter 2 of this work. In the second step, the specific dimensions of the cross section must be defined, as illustrated in Figure 6. The following section provides a comprehensive examination of the analytical methods employed and the corresponding results generated by the program.

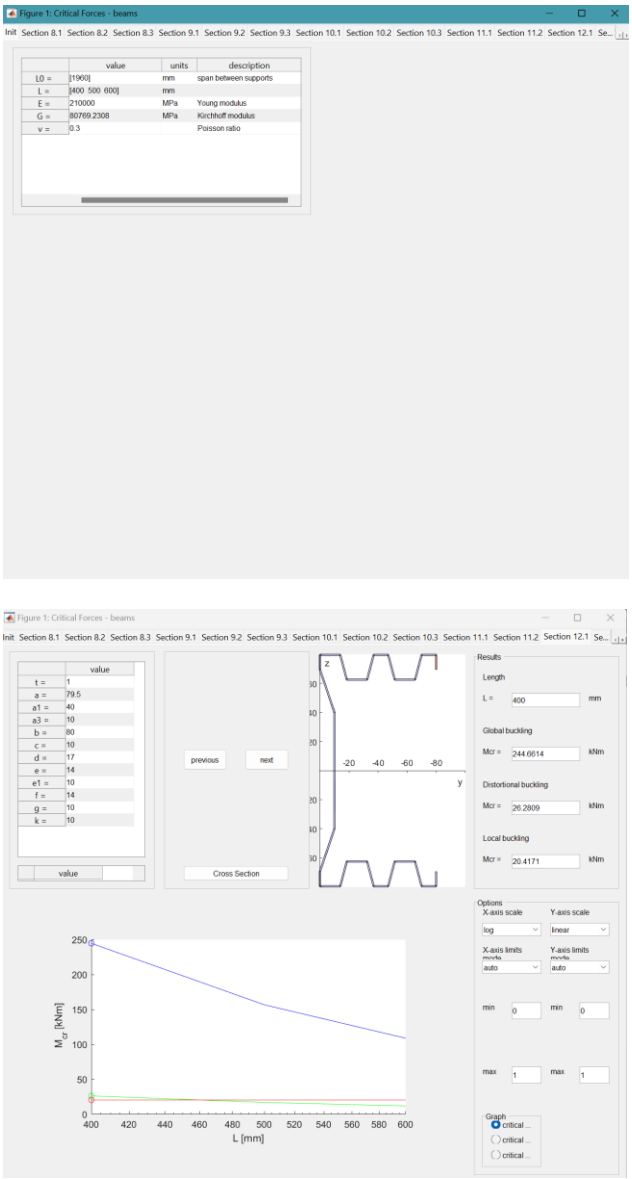

Fig. 6. Interface of the program for calculating critical moments of bent beams, developed by Dr. Marcin Rodak using the analytical formulas from this chapter

For the lengths specified in the first step, the program calculates the critical moments based on Eq. (11), Eq. (20), and Eq. (24). An essential aspect of using this program is understanding the buckling mode to which each beam is susceptible. The program computes critical moments for global, distortional, and local buckling modes. All results generated by the program are presented in the results Table 2. For the final comparison with results obtained from other methods, the value corresponding to the buckling mode identified in the experimental tests was selected. This ensures that the most relevant and accurate data are used for comparison and analysis.

The results of the analytical calculations are shown in Table 3. The values of critical moments for the corresponding forms of beam buckling are indicated: B1 and B3 - local, B5 - distortional. Different beam lengths L, i.e. 400, 500, 600, 700 and 800 mm and three different plate thicknesses t, i.e. 1.4 mm, 1 mm and 0.6 mm, were taken into account.

TABLE 2. Results of the analytical calculations

Beam	Critical moments $M_{cr}[kNm]$		
	B1	B3	B5
Length L $[mm]$	**400**		
$t = 1.4mm$	6.25	6.32	25.84
$t = 1mm$	2.28	2.30	18.22
$t = 0.6mm$	0.49	0.50	10.83
Length L $[mm]$	**500**		
$t = 1.4mm$	6.26	6.33	16.78
$t = 1mm$	2.28	2.31	11.75
$t = 0.6mm$	0.49	0.50	6.95
Length L $[mm]$	**600**		
$t = 1.4mm$	6.27	6.35	11.86
$t = 1mm$	2.29	2.31	8.23
$t = 0.6mm$	0.49	0.50	4.84
Length L $[mm]$	**700**		
$t = 1.4mm$	6.25	6.33	8.90
$t = 1mm$	2.28	2.31	6.12
$t = 0.6mm$	0.49	0.50	3.57
Length L $[mm]$	**800**		
$t = 1.4mm$	6.25	6.32	6.97
$t = 1mm$	2.28	2.30	4.74
$t = 0.6mm$	0.49	0.50	2.75
Buckling form	Local	Local	Distortional

For beams B1 and B3, which are subject to local buckling, the critical moment remains constant regardless of the beam's length. This occurs because, as the beam length increases, the difference between the actual buckling half-wave length and the half-wave length associated with the smallest critical moment decreases. Consequently, for longer beams, the critical moment for local buckling stabilizes and does not vary with changes in length. This behavior is a characteristic feature of local buckling in thin-walled structures, where the buckling wavelength is largely independent of the overall beam length once a certain threshold is reached.

As previously mentioned, for beams experiencing local loss of stability, the critical moment remains constant regardless of the distance between supports. This constancy underscores the fact that local buckling is primarily governed by the geometry of the cross-section rather than the beam length. However, this is not the case for beam B5, which is subject to distortional instability. In this instance, the critical moment decreases as the beam length increases, reflecting the more complex nature of distortional buckling, where both cross-sectional and length factors play significant roles.

Furthermore, an analysis of the effect of plate thickness on the critical moment reveals that the critical moment decreases with a reduction in plate thickness. This relationship holds true across all the beams tested, emphasizing the importance of material thickness in resisting buckling. Among the tested beams, beam B5 demonstrated the highest critical moment with a support length of 400 mm and

a plate thickness of 1.4 mm. This result highlights the interplay between length, thickness, and buckling mode, illustrating how these factors collectively influence the structural performance of the beams under load.

4. FINITE ELEMENT METHOD

This chapter presents the results of numerical analyses performed using the finite element method (FEM) to investigate the behavior of the beams under study. The ANSYS software was employed to conduct these simulations, providing a detailed insight into the structural response of the beams under various loading conditions. The following sections outline the methodology, boundary conditions, and material properties used in the simulations, as well as a discussion of the key findings obtained from the FEM analysis. Through these numerical analyses, a deeper understanding of the critical factors influencing the stability and performance of the beams is achieved, complementing the analytical calculations presented earlier.

4.1. FE model of the beam and boundary conditions

Numerical analyses were performed using finite element method within ANSYS software. The procedures for linear and non-linear calculations available in this system were used. To model all beams the DesignModeler has been used that is a part of ANSYS. Since the buckling mode and the mode of failure may have an asymmetric form a whole beam has been modelled although the geometry, load and support conditions were symmetrical. It was decided to abandon modelling the bending radii having in mind that in actual beam the strain hardening effect may influence the behaviour of the beam by increasing its stiffness. Straight corners on the cross-sections of the FE models prevent from generation of small, distorted finite elements which could appear on the bending radii and adversely affect the numerical solution.

A pure bending load conditions has been applied to the model which is a typical load for testing structural elements like beams. Since the effect of such load is to be achieved in the simplest possible way without reproducing the test stand a number of simplifications have been made. Only a central part of the beam has been modelled which undergoes a pure bending. The bending conditions were achieved by adding rigid plates at both ends of the model (see figure 7) and by applying forces to the upper and lower edge of the plates, compressive and tensile one, respectively. The Young modulus of rigid plates are 10^3 times higher than the one for the beam. A similar solution has been used in paper by Jasion et al. [8].

A pure bending load conditions has been applied to the model which is a typical load for testing beams. The bending conditions were achieved by adding rigid plates at both ends of the model (see figure 7) and by applying forces to the upper and lower edge of the plates, compressive and tensile one, respectively. The model was supported along the line at mid-height of the rigid plate in the way that the displacements in the y and z direction were blocked. Additionally, to avoid a rigid body motion, the displacement in the x direction was blocked at one node on the vertical symmetry plane of the beam. Between the beam and the rigid plates the contact conditions have been defined in the form of bonding connection.

The whole model of the beam has been covered with a second order shell elements shell281 with 8 nodes and 6 DOF in each node. This element is suited for modelling thin shell-like structures for linear elastic analyses but also for structures undergoing large strains and large rotations in non-linear analyses. It can be also related with plastic properties of the material model. The size of the finite element has been chosen based on the convergency analysis the results of which are shown in figure 5d. The size is equal to 5 mm which is a compromise between the computational time and the precision of the results. Additional condition about the element size has been imposed on the perforated web to obtain finer mesh, about 2 mm size of the element, around the circular holes. No special effort on the mesh around the holes was paid since the deformation of the perforated web is slight and has the form of mild buckling waves. The deformation is even smaller in the non-linear analyses since here mostly flange undergoes deformation. Moreover a circular shape of the holes prevents from arising local stress concentrations.

The convergency analysis has been performed for two beams. One of them had a flat flange, beam B3, and the second one had a corrugated flange, beam B5. The parameters which have been analyzed during calculations were the critical bending moment, the left vertical axis, and the normal stress measured in the mid-length of the upper flange, the right vertical axis. To simplify the reading of the plots the power trend lines have been added to each set of the data.

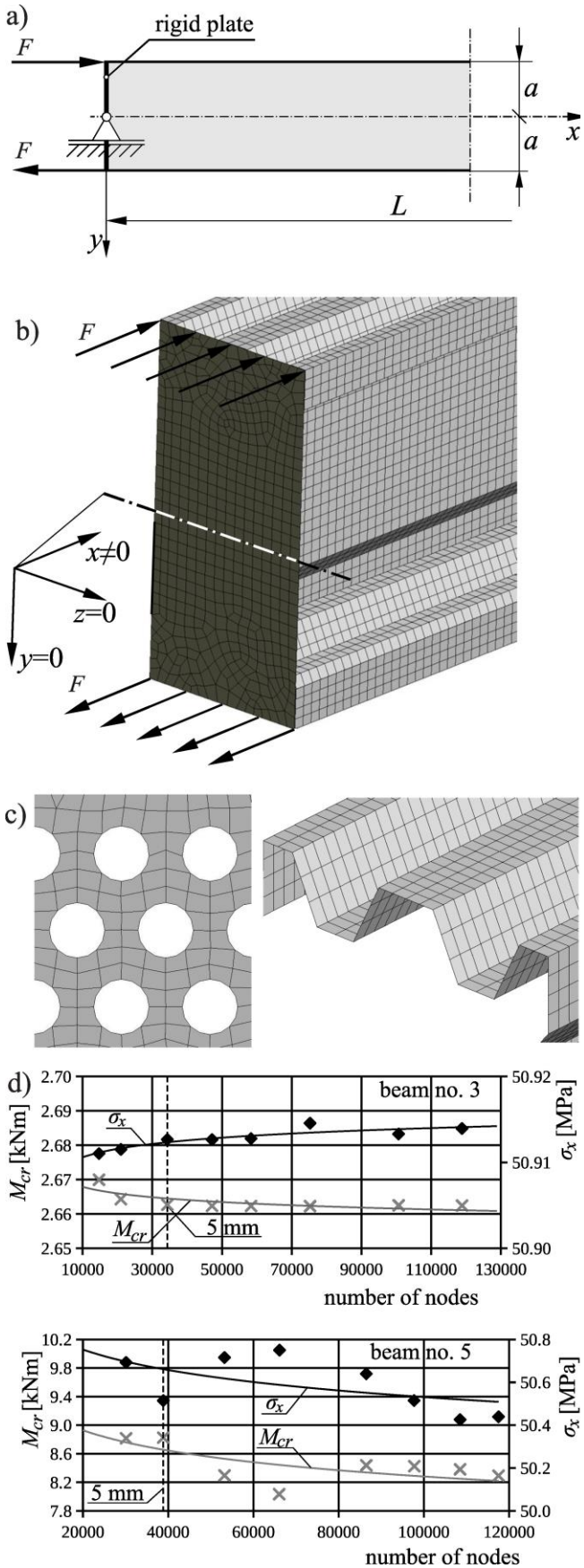

Fig. 7. Details of FE model: a) model of the beam under pure bending; b) boundary conditions; c) mesh pattern around the holes of perforation and on the corrugated flange; d) results of the convergency study

In the case of the beam with a flat flange the size of the finite element does not influence the results almost at all. The decrease the size of the element results in the change of the analysed parameters only about 0.3%. For the beam B5 the results are not so smooth which can be explained in two ways. First of all due to the shape of the corrugation the relation between the size of the element and the number of elements is not smooth. Second, the buckling mode has a local character and the change of the location of the waves may change the buckling load in a distinctive way. However, if the values on the vertical axes are observed, the stress varies within the range of 0.5%, and the buckling load within the range of 6%. Thus the selected size of the element seems to be enough having in mind that the main goal of the analyses is to determine the critical and limit load. The precise analysis of a local phenomenon like the local fold in the plastic range would need further improvements in the model.

For the linear buckling analysis a linear elastic material has been modelled with the following parameters: Young's modulus $E = 185000\,MPa$, Poisson's ratio $\nu = 0.3$ and the mass density $\rho = 7850\,kg/m^3$. For the post-buckling analysis the bilinear elastic-perfect plastic model has been assumed with the yield strength $R_{eH} = 328\,MPa$. The stiffened plates attached at both sides of the beam have been modelled using the same material, a linear elastic one, but its stiffness, that is the Young's modulus, is 10 times this of the material of the beam. The thickness of these plates equal 10 mm.

After accepting the results of the convergency study the validation process has been made on the model of the beam to determine how accurately it reflects the behaviour of an actual beam. First the flat specimen has been modelled to which the material properties have been ascribed as listed above. The geometry of the model corresponds to this of an actual specimens presented in figure 1. The comparison of the FE results with four plots obtained from experiments is provided in figure 9a. It is seen that in the elastic range the behaviour of the material and its model is the same. Also the plastic flow starts at about the same value of the load. On the plot only its initial part is provided since it seems to be enough having in mind that the goal of the investigation is the determination of the buckling and limit load.

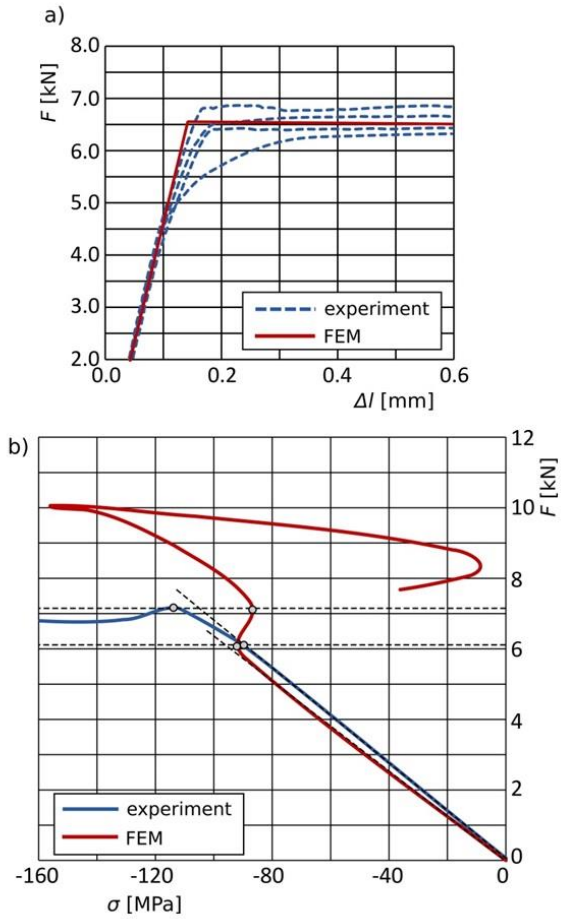

Fig. 8. Validation of the FE model of the beam: a) static tensile test of the material; b) stress in the web of the beam under bending

As a second step of the validation the normal stress in the web of the B1 obtained from the strain gauge measurements has been compared with the stress determined in the FE analysis (see figure 8b). The difference in the initial stiffness manifested by a different slope of the paths is acceptable remembering that the FE model is not intended to reproduce the test stand but is simplified to provide a pure bending condition in a simple way. The most important information is points marked on both curves which correspond to following stages of the loss of stability and deformation. For both curves they are at about the same level of load. The lower value indicates the initial loss of stability and the higher one is related to the start of formation of a local folding. Although the curves differ after the second point is exceeded the results are acceptable because the goal was to determine the limit load. The differences in the shape of the two curves are the result of the final failure mode shape. In the case of the FE model the a purelocal fold appeared near the mid-length of the beam where the stresses were read and thus their changes were seen when the fold on the web and then on the flange were formed. In experiment in contrast the failure taken place near the support giving more gentle curve.

4.2. Influence of the length, thickness and perforation on the buckling behaviour

The first type of analysis performed to investigate the buckling resistance of beams was the linear buckling analysis. Due to it one may analyse the influence of the geometry of the cross-section, the thickness of the sheet-metal and the length of the beam on the value of the buckling load and the corresponding buckling mode.

This analysis also gives the possibility to compare the beams with different cross-sections and indicates the way to improve the buckling resistance of such structures. In the present investigation there are three different cross-sections investigated, however, each of them exists in two different versions – with a solid web and with the web containing perforation in the form of small holes. For each pair of beams a separate plot has been prepared on which the relation between the length of the beam and the critical bending moment is shown. Three pairs of curves correspond to three different thicknesses of the sheet-metal used to model the beam.

In the case of beams B1 and B2 the buckling shape has the same character – the waves appear on the web, flange and the lip (see figure 9). The character is similar for all analysed thicknesses and lengths. The difference is in the number of waves. From the plot shown in figure 9 it is seen that the perforation decreases the buckling load by 10% with the loss of the weight about 14%. The reason for that is that the buckling waves appear also on the web the stiffness of which is reduced due to perforation.

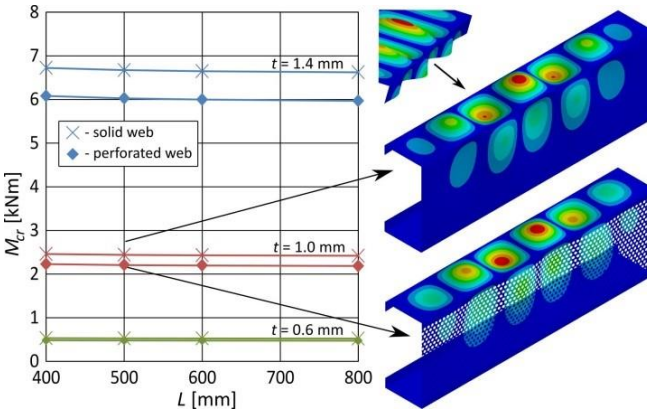

Fig. 9. Results of buckling analysis for beams B1 and B2

For beams B3 and B4 (see figure 10) the buckling load has the form of short waves which appear on the flange and the lip. The web remains flat due to corrugation which increases its stiffness. As an effect the value of the buckling load for both types of beams is very similar. The perforation decreases this value only about 1.5% whereas the mass of the beam is decreased about 8%.

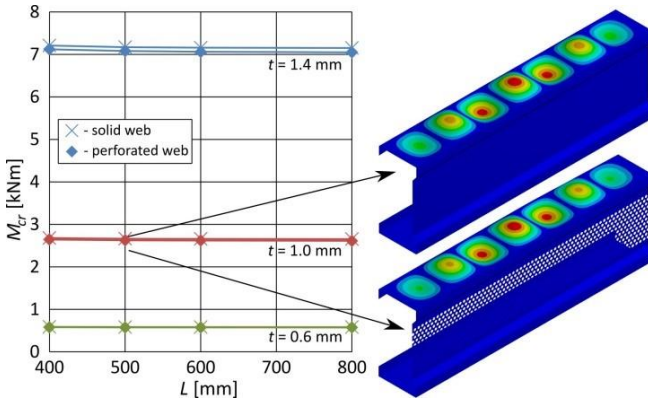

Fig. 10. Results of buckling analysis for beams B3 and B4

The relation between the length and the thickness of the sheet-metal, and the buckling behaviour of beams B5 and B6, shown in figure 11, is more complex than for previously analysed cases. For longer beams made of thicker sheet-metal a global buckling mode appears in the form of one half-wave encompasses the whole upper flange. These cases are marked in figure 11 with circles. For other beams the local phenomenon appears in the form of short waves located on the lip. The dashed line on the plot corresponds to the buckling load which has local character (2nd and 3rd buckling modes).

From the results it follows that for beams which buckle in a global way the corrugation decreases the buckling load up to 2%. For the beams which buckle locally this decrease reaches about 1%. The weight of the beam due to perforation has decreased about 17%.

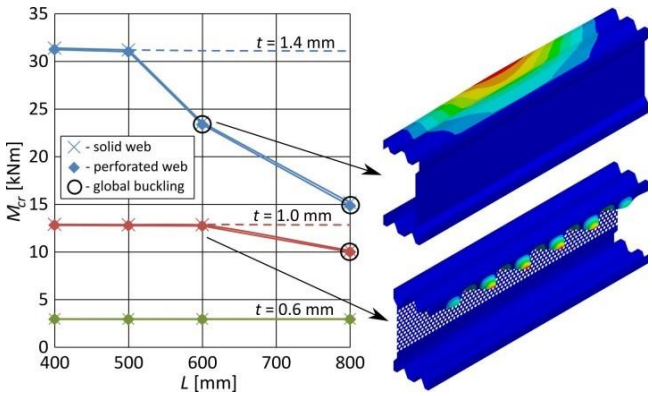

Fig. 11. Results of buckling analysis for beams B5 and B6

It is also worth to notice that the value of the linear buckling load for beams B1 to B4 do not depend on the length of the beam in a significant way. The differences between the values for the shortest and the longest beam do not exceed 2%. Similar results can be observed for beams B5 and B6 which buckle locally. The influence of the length parameter on the buckling load is clearly visible for beams which buckle in a global way. This can be explained by the fact that there is only one half-wave spread on the whole length of the flange and in such a case this length influence considerably the buckling resistance. The critical moment for the longest beam is 52% smaller than for the shortest one for $t = 1.4\,mm$ and 22% for $t = 1.0\,mm$. Some additional attention should be paid for the longest version of beams B5 and B6 for which $t = 1.4\,mm$. The first buckling mode is a global one and the corresponding buckling load equals about 15 kNm. However, if it would be possible to enforce a local buckling (third buckling mode) the load could be increased about 109%.

4.3. Comparison of beams with different cross-sections

Additional comparison have been prepared for all cross-sections considered in investigations. This way the influence of the modifications of the shape of the cross-section on the buckling resistance of the beam can be analysed. Two families of beams have been investigated: the first one of the length $L = 500\,mm$ and the second one of the length $L = 800\,mm$. The results are presented in figure 12 in the form of relation between the sheet-metal thickness and the critical moment.

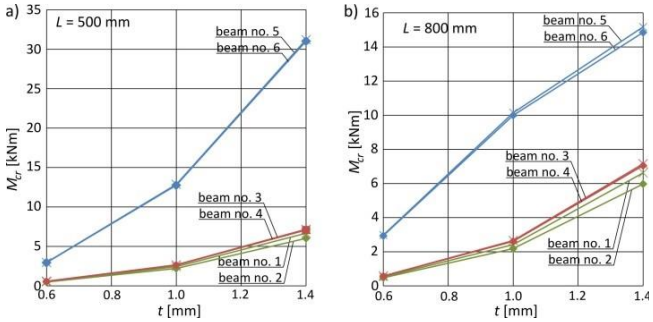

Fig. 12. Comparison of buckling loads of beams with different cross-sections: a) beams with the length equal to 500 mm; b) beams with the length equal to 800 mm

As can be expected since the deformation of the beams due to buckling is concentrated on the flange the modification of this part of the beam gives the highest increase in buckling resistance. Depending on the sheet-metal thickness the buckling strength is about 1.2 to 4.7 times higher for beams B5 and B6 than for other beams. The modification of the web provides the increase of the buckling load about 7 to 11% when beams B1 and B3 are compared, depending on the thickness parameter.

4.4. Parametric study

The shape of the cross-sections of beams investigated in this paper has been based on the results of previous analyses, the experience of the authors and most of all they were limited with the manufacturing process. However, to show a broader view of the influence of this shape on the buckling behaviour of the beam the parametric study has been conducted for the beam B5. Two parameters have been introduced to control the geometry of the cross-section. The first one is the width of the base of the trapezoid in the flange f_1, and the second one – the width of the base of the trapezoid in the web f_2 (figure 13j).

For the parameters equal to $f_1 = 19.75\,mm$ and $f_2 = 61.5\,mm$ the cross-section takes the form of the classical lipped channel as shown in figure 13g which is a reference shape for this study. If both parameters equal zero the most extreme case is obtained shown in figure 13c. Other parameters describing the cross-section are provided in figure 13j. The dimensions a, w, and d are the same as in the analyses presented in previous sections. Additionally an angle parameter α has been introduced the value of which equals 30°.

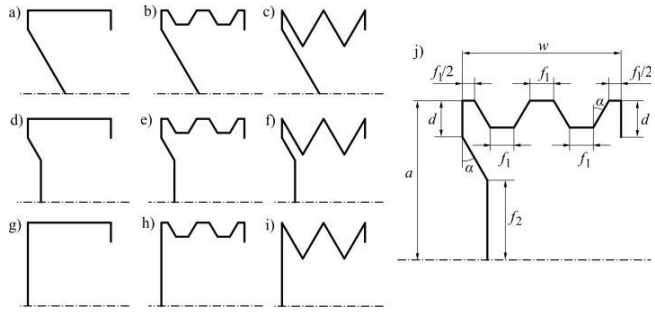

Fig. 13. Exemplary shapes of cross-sections of beams (a-i); geometrical parameters of the cross-section (j)

The finite element model is the same as in the previous analyses. Only one length of the beam has been taken into account that is $L = 500\,mm$. The thickness of the reference shape is equal to $t = 1.4\,mm$. Thicknesses for other shapes have been determined in the way to keep the weight of the beam equal to the weight of the reference beam which is approximately 1.94 kg. Thicknesses of sheet-metal for all analysed models are provided on Table 3 along with the values of the critical bending moments corresponding to the first buckling mode.

TABLE 3. Buckling loads and thickness of beams

$f_2\,[mm]$														
	0.0	$t\,[mm]$	1.328	1.307	1.280	1.229	1.182	1.139	1.098	1.060	1.025	0.992	0.961	0.932
		$M_{cr}\,[Nm]$	6429.7	9221.5	13071	15447	18259	17199	14970	12729	10703	9176.4	8470.1	8497.0
	8.0	$t\,[mm]$	1.337	1.316	1.288	1.237	1.189	1.145	1.104	1.066	1.031	0.997	0.966	0.937
		$M_{cr}\,[Nm]$	6558.9	9354.0	13148	15625	18372	17058	15050	12794	10759	9207.8	8345.0	8679.2
	16.0	$t\,[mm]$	1.346	1.325	1.297	1.245	1.196	1.152	1.110	1.072	1.036	1.002	0.971	0.941
		$M_{cr}\,[Nm]$	6698.8	9504.1	13468	16010	18776	17754	15453	13169	11073	9491.7	8777.8	8838.0
	24.0	$t\,[mm]$	1.355	1.334	1.305	1.252	1.204	1.158	1.117	1.078	1.041	1.007	0.976	0.946
		$M_{cr}\,[Nm]$	6837.5	9658.1	13778	16372	19156	18147	15854	13492	12324	9715.5	8987.6	9053.3
	32.0	$t\,[mm]$	1.365	1.342	1.314	1.260	1.211	1.165	1.123	1.083	1.047	1.012	0.980	0.950
		$M_{cr}\,[Nm]$	6983.6	9784.5	14133	16770	19533	18603	16237	13796	11618	9945.3	9174.5	9241.6
	40.0	$t\,[mm]$	1.374	1.352	1.323	1.268	1.218	1.172	1.129	1.089	1.052	1.018	0.985	0.955
		$M_{cr}\,[Nm]$	7103.2	9940.0	14488	17116	19885	19031	16596	14116	11868	10195	9381.0	9449.5
	48.0	$t\,[mm]$	1.384	1.361	1.331	1.276	1.226	1.179	1.136	1.095	1.058	1.023	0.990	0.959
		$M_{cr}\,[Nm]$	7217.4	10092	14716	17232	20093	19411	16951	14406	12129	10404	10534	9621.2
	56.0	$t\,[mm]$	1.393	1.370	1.340	1.285	1.233	1.186	1.142	1.101	1.063	1.028	0.995	0.964
		$M_{cr}\,[Nm]$	7246.9	10228	14421	16822	19776	19745	17218	14656	12331	10593	9763.7	9811.3
	61.5	$t\,[mm]$	1.400	1.377	1.347	1.290	1.239	1.191	1.147	1.106	1.067	1.032	0.998	0.967
		$M_{cr}\,[Nm]$	7050.4	9396.3	12842	11464	11731	9946.7	8939.3	7977.0	6646.4	5996.8	5679.9	5557.1
			19.75	19.00	18.00	16.00	14.00	12.00	10.00	8.00	6.00	4.00	2.00	0.00
			$f_1\,[mm]$											

From Table 3 it is seen that the highest buckling load equals 20.09 kNm and corresponds to the beam characterised by parameters $f_1 = 14\,mm$ and $f_2 = 48\,mm$. Thickness of the corresponding sheet-metal equals 1.226 mm. The corresponding cross-section is provided in figure 14a.

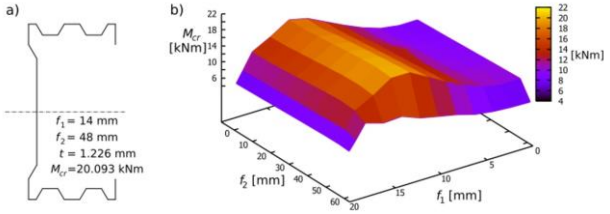

Fig. 14. Buckling loads for beams from parametric study a); cross-section with the highest buckling resistance b) critical moment as a function of f_1 and f_2

To simplify the analysis of the results the plot has been prepared based on the Table 3 which is shown in figure 14b. Looking at the plot it is seen that the parameter f_1 has much higher influence on the buckling resistance of the beam than the parameter f_2. The value of the buckling load for a given value of f_1 changing only slightly for different values of f_2. For example for $f_1 = 14\,mm$ the difference between the highest and lowest value equals 1.8 kNm which is 9.1% of the highest value. For $f_1 = 2\,mm$ the difference reaches 20.8% and is the biggest one. If similar calculations are made for selected values of the parameters f_2, the differences are between 50 and 55%. The variants with flat web and flat flange were omitted in this calculation. The fact that the parameter f_2 does not influence the buckling resistance of the beam significantly is directly related to the buckling modes which, for selected beams, are shown in figure 15. For a given value of f_1 the mode remains roughly the same for all values of f_2.

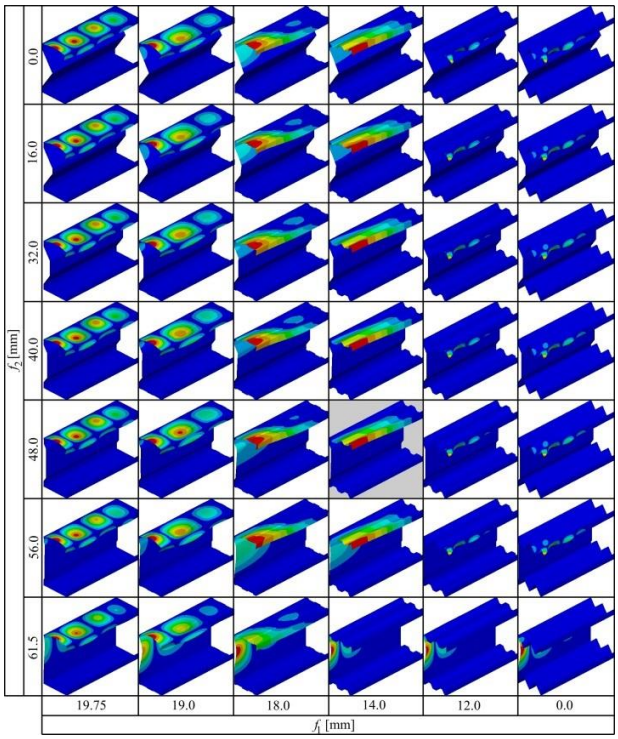

Fig. 15. Buckling modes of selected beams

Analysing the table from figure 15 it can be seen that for initial configuration, the buckling mode has the shape of short waves located on the web, flange and the lip (bottom left corner). If the corrugation of the flange increases (f_1 decreases) the flange becomes stiffer and the waves are concentrated on the web. Similar situation can be observed for the web – for higher corrugation (smaller values of f_2) the waves disappear from the web. For small values of both f_1 and f_2 the buckling mode has the form of short waves located on the lip only. The highest value of the buckling load corresponds to the buckling mode in the form of one half-wave located on the upper flange. This observation suggests that further increase of the buckling resistance can be achieved by increasing of the stiffness of the flange.

4.5. Limit load

When thin-walled beams are to be used as structural elements it is necessary to investigate their post-buckling behaviour and to determine the load at which the beam loses its load capacity. For this reason the non-linear analysis has been performed using the arc-length method which apart from the limit load gives the possibility to analyse the way the beam will collapse. A large deflection effect was applied. The model was loaded with the forces acting the same way as in the linear buckling analysis and the convergence parameter was the force the value of which was controlled by the system. The initial imperfections introduced into the model had the form of the first eigenmode obtained from the linear buckling analysis and their magnitude were equal to 1% of the sheet-metal thickness.

Two types of non-linear models have been created. The first one was a geometrically non-linear model in which the linear elastic behaviour of the material was assumed. The second one was a geometrically and materially non-linear model. In the latter case the elastic-perfectly plastic model of the material has been used. The second model gives the possibility to predict the maximum load the beam can be loaded with before the plastic deformation appears.

The analyses have been performed for each of six beams. The initial imperfections introduced into the model had the form of the first eigenmode obtained from the linear buckling analysis and their magnitude were equal to 1% of the sheet-metal thickness. The results are presented in the form of equilibrium paths. The horizontal axis corresponds to the maximum displacement normalized by the sheet-metal thickness whereas the vertical axis corresponds to the dimensionless bending moment which is the bending moment applied during the analysis divided by the critical moment. To the plots the pictures have been added on which the deformation is shown for the case of the elastic material and for the case of plastic material, apart from the deformation, the equivalent plastic strain distribution is provided. Additionally, to have the possibility to compare the numerical results with the results of experiments, the equilibrium path has been provided in which the applied moment versus the displacement of the point located in the mid-length of the upper flange is shown.

When comparing the paths presented in Figures 16 to 21 two different behaviours can be distinguished. For

beams B1 to B4 the flange of which is flat, the critical load is slightly below the buckling load determined in linear buckling analysis for both models of the material. Initially, after the buckling load is exceeded, the paths for both materials' models overlap each other which suggests that the buckling appears in an elastic range. After that, at about 1.4 of the critical load the paths start to separate. For elastic material the buckling waves located on the upper flange and the lip increase. For the elastic-plastic material, after the plastic limit is reached the deformation starts to increase locally and the collapse of the beam can be observed.

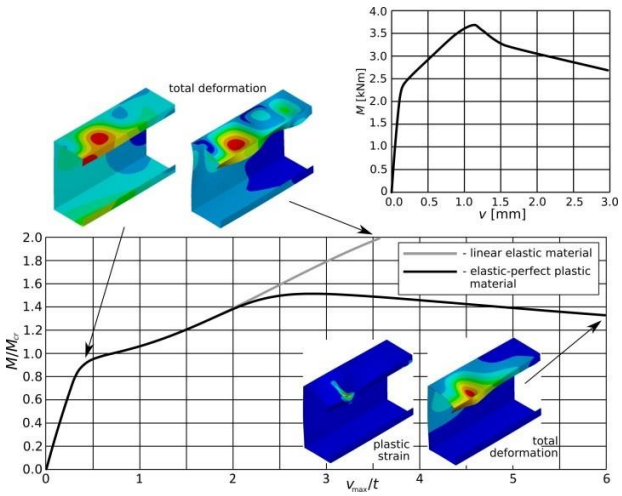

Fig. 16. Equilibrium path for the beam B1

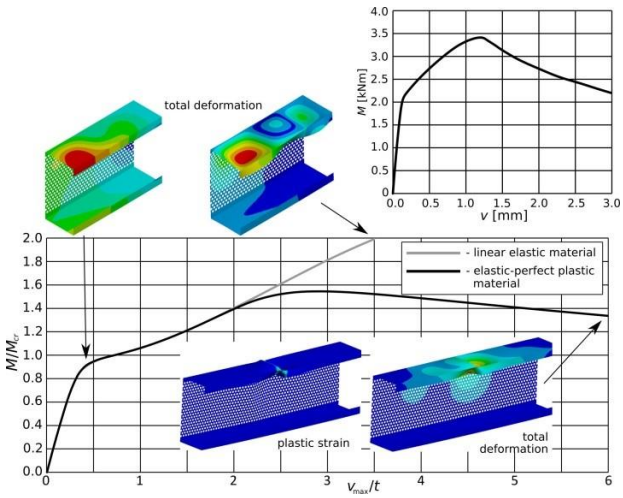

Fig. 17. Equilibrium path for the beam B2

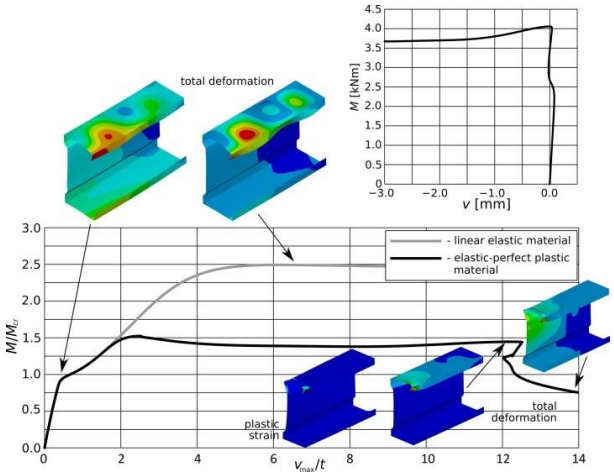

Fig. 18. Equilibrium path for the beam B3

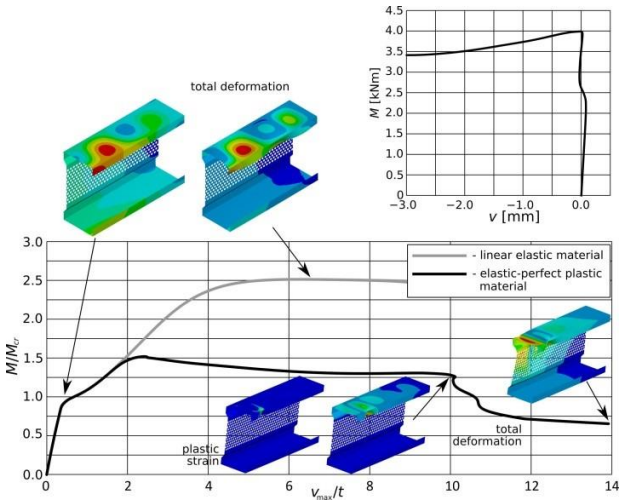

Fig. 19. Equilibrium path for the beam B4

Different behaviour can be observed for beams B5 and B6 which have a corrugated flange. Due to the corrugation the buckling load for these beams is much higher than for the other beams. The consequences are that the stresses reach much higher values and before the buckling appears the material starts to flow plastically. It is seen on plots in Figures 17 and 18 that the limit load for these beams is about 50% of the linear buckling load.

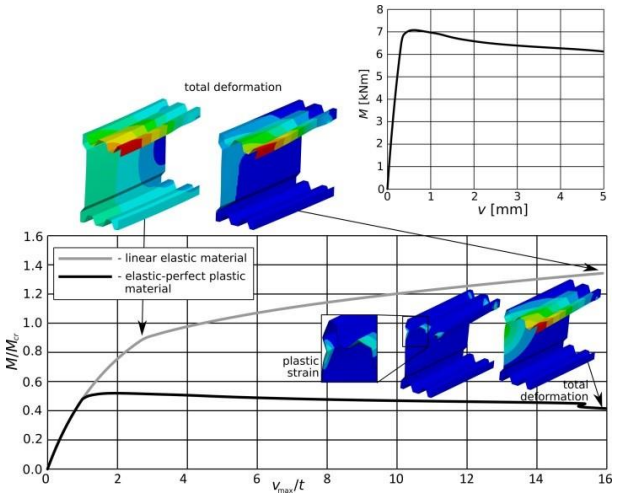

Fig. 20. Equilibrium path for the beam B5

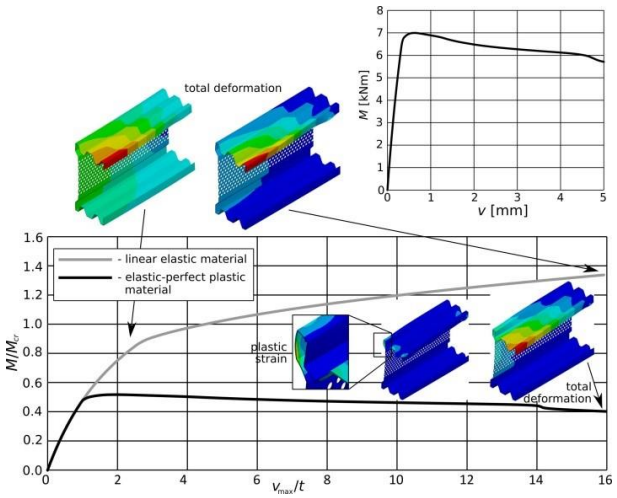

Fig. 21. Equilibrium path for the beam B6

The total deformation for beams B5 and B6 in the non-linear analysis is the same for both materials' models adopted and has the global form. It is similar to the buckling mode obtained in the linear analysis but in addition to the flange deformation in the form of one half-wave the web also deforms.

5. COMPARISON AND CONCLUSION

In the following section, the research results will be presented, encompassing both experimental findings and finite strip analyses that were thoroughly detailed in the first part of this article. Additionally, this section will incorporate results derived from analytical solutions and finite element analyses. Together, these diverse methodologies provide a comprehensive understanding of the structural behavior of the thin-walled beams under investigation, yielding valuable insights into their stability and load-bearing capacity.

The primary objective of this research was to assess the impact of web perforations on buckling modes, stability resistance (critical force), and ultimate load-bearing capacity (maximum force). The critical force values obtained from all four methods are presented in Table 4.

TABLE 4. Critical forces [kN], EXP – experimental tests, FSM – inite strip method, AC – analytical calculations, FEM - finite element method

Beam	$F_{cr_{EXP}}$	$F_{cr_{FSM}}$	$F_{cr_{AC}}$	$F_{cr_{FEM}}$
B1	6.00	5.07	4.60	4.80
B2	5.10	-	-	4.20
B3	5.00	5.67	4.60	5.40
B4	6.50	-	-	5.20
B5	14.90	31.49	23.60	13.80
B6	11.20	-	-	13.60

Beams B1 and B2, with the classic lipped channel cross-section, served as reference points for comparing the stability results of beams with modified cross-sectional shapes. As cross-sectional complexity increases, critical force values also increase, indicating improved resistance to stability loss. The highest critical force values were obtained for the beams with trapezoidal flanges (B5 and B6), emphasizing that modified geometries positively impact stability. Quantitative analysis shows that beam B5, with a solid, flat web, offers nearly 2.5 times the stability of the classical B1 cross-section, underscoring the benefits of cross-sectional modifications on stability.

Perforations in the web lead to a significant reduction in critical force values, which negatively impacts the beams' resistance to loss of stability. However, when evaluating the effect of perforations on structural performance, the reduction in weight of the beams plays a crucial role. Beams with perforated webs are lighter than those with solid webs, which is a significant advantage. Table 5 presents a dimensionless comparison of the critical force relative to the beam's weight, and the purpose of this analysis is to determine whether the percentage reduction in weight outweighs the slight decrease in critical force.

TABLE 5. Non-dimensional critical forces with corresponding beam weights

Beam	Weight [kg]	$F_{cr_{EXP}}$ $[kN]$	$F_{cr_{FEM}}$ $[kN]$
B1	5.19	6.00	4.80
B2	4.40	5.10	4.20
B1/B1	1.00	1.00	1.00
B2/B1	**0.85**	**0.85**	**0.88**
B3	5.25	5.00	5.40
B4	4.78	6.50	5.20
B3/B3	1.00	1.00	1.00
B4/B3	**0.91**	**1.30**	**0.96**
B5	6.31	14.90	13.80
B6	5.85	11.20	13.60
B5/B5	1.00	1.00	1.00
B6/B5	**0.93**	**0.75**	**0.99**

For the dimensionless comparison, beams with solid, flat webs served as the reference cross-section for each pair. Evaluations were conducted separately for each pair, leading to the following conclusions:

- In beams B1 and B2, the perforated beam's weight decreased by 15%, accompanied by a 15% reduction in critical force.
- For beams B3 and B4, the perforated beam's weight reduced by 9%, while the critical force increased by 30%.
- In the comparison of beams B5 and B6, the perforated beam's weight decreased by 7%, yet the critical force significantly dropped by 25%.

For pairs B1/B2 and B5/B6, the decrease in weight correlated with the expected reduction in critical force. However, for beams B3 and B4, the perforated beam exhibited a significant increase in critical force despite a weight reduction. Finite element analysis indicated that the critical force for beam B4 (perforated) decreased by only 4% compared to beam B3 (solid, flat web). Thus, in this case, the benefits of using perforations are evident, as the weight reduction outweighs the minor decrease in critical force.

In the analysis of thin-walled structures, geometric imperfections significantly impact their resistance to loss of stability.

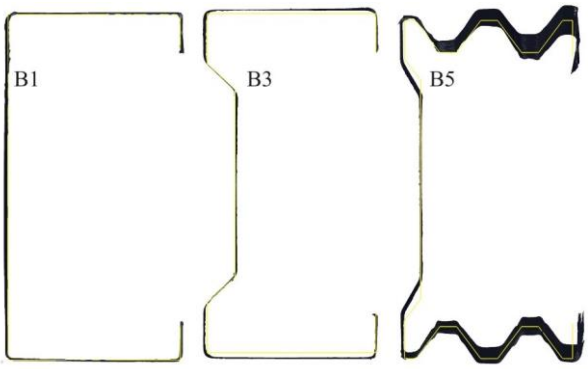

Fig. 22. Geometric imperfections of the cross sections of the beams

Figure 22 illustrates the geometric imperfections in beams B1, B3, and B5. The yellow color represents the ideal CAD dimensions, while the black line indicates the shape deviations projected onto the cross-sectional view along the entire length of the beam. Beam B5 exhibits the most significant deviations. These geometric imperfections notably affect the stability and load-bearing capacity of bent beams and compressed columns, as shown in the study by Pawlak et al. [30].

An important innovation in this work is the modification of the beam cross-sectional shape, which significantly increases both critical and maximum forces, enhancing structural performance. Additionally, while web perforations cause a slight reduction in critical force, they lead to a considerable weight reduction, providing efficiency gains with minimal impact on stability.

6. SUMMARY

In this part of the article, conclusions from analyses conducted using four methods - experimental studies, Finite Strip Analysis (FSM), Finite Element Analysis (FEM), and analytical calculations - are presented. This broad spectrum of methodologies enabled mutual verification of results, which was crucial given the unique combination of cross-sectional shape modifications and perforations in the beams analyzed. The lack of references in the literature for such constructions necessitated additional accuracy and validation, provided by the multi-method approach.

- Modifying the cross-sectional shape, as a significant innovation, increases both the maximum load capacity and the critical force; a more modified shape results in a higher critical force, positively influencing the structure's overall stability.
- Perforations in the web significantly reduce beam weight, enhancing material efficiency and cost savings in lightweight design. Critical force values, crucial for thin-walled structure analysis, decrease slightly relative to weight reduction, indicating a favorable compromise between stability and mass.
- The use of perforations balances the goal of minimizing structure mass while maintaining high strength. This approach responds to the increasing demand for lightweight yet durable structural solutions.
- The studies demonstrated that regardless of whether the beams had a solid, flat web or were perforated, they experienced local loss of stability. This instability mechanism was documented in both experimental analyses and numerical simulations conducted using the FEM.
- The influence of geometric imperfections in thin steel sheets is significant, and discrepancies in results may stem from these imperfections, affecting stability and load capacity. The authors are currently undertaking a research project focused on analyzing the impact of geometric imperfections on the strength and stability of thin-walled steel elements, aiming for improved understanding and design recommendations.

NOTIFICATION

$\boldsymbol{k_y, k_z, k_\psi}$ – spring rates in the flange model for distortional buckling

J_y, J_{yz}, J_z – moments of inertia of the cross-section
u, v, w – shear center displacement S
u_R, v_R, w_R – displacement components of the point R
x, y, z – basic beam coordinate system
$x, \bar{y}, \bar{z}$ – central coordinate system connected to the flange of beam with the middle at point $\bar{C}$
$\beta_{sz}, \beta_{sy}, \beta_\omega$ – Wagner's coefficients
x, η, ς – local coordinate system
M_y, M_z – bending moments about y and z axes
y_R, z_R – coordinates of the point R, lying at one end of the midline of the wall
y_s, z_s – coordinates of the shear center S
A – cross-sectional area of the beam
B – bimoment
C – center of gravity of the beam cross-section
$\bar{C}$ – center of gravity of the flange
C' – displaced center of gravity of the beam cross-section for overall buckling
E – Young's modulus
F_{cr} – critical force
G – Kirchhoff modulus
J_t - the Saint-Venant torsion constant
J_ω – warping constant
L – the length of the middle span subjected to pure bending
L_c – total length
L_0 – distance between supports
L_s – distance between applied force and supports
M_{cr} – critical moment
M_g – bending moment
N – axial force
r_S^2 – polar radius of inertia about the shear center S
$R_{eH} = f_{yb}$ – yield strength
$R_m = f_u$ – ultimate strength
t – thickness
U_ε – elastic deformation energy
$U_{\varepsilon n}$ – nonlinear elastic deformation energy
$U_{\varepsilon l}$ – linear elastic deformation energy
W – work of external forces
$\tilde{w}$ – the deflection of the wall towards ζ
$\bar{z}_C$ – the coordinate of the beam section center in the coordinate system associated with the flange
κ – the coefficient depending on the ratio of wall dimensions $\lambda = \frac{L}{h}$ and parameter β
κ_{cr} – the critical coefficient depending on the ratio of wall dimensions $\lambda = \frac{L}{h}$ and parameter β
λ – slenderness of the beam
ν – Poisson's ratio
ρ – mass density
σ_g – bending stress
σ_x – normal stress in the x-axis direction
ψ – torsion angle
ψ_1 – dimensionless parameter

ACKNOWLEDGEMENTS
The project was funded by the National Science Centre, Poland allocated on the basis of the decision No. DEC-2021/43/B/ST8/00845 of 2022-05-23 – Contract No. UMO-2021/43/B/ST8/00845.

REFERENCES

[1] K. Rosłaniec and P. Różyło, "Stability of Thin-Walled Composite Structures with Closed Sections Under Compression," *Advances in Science and Technology Research Journal*, vol. 18, no. 3, pp. 188–199, 2024, doi: 10.12913/22998624/186473.

[2] Z. Bakhach, A. El Kaimbillah, A. Hamdaoui, B. Braikat, F. Mohri, and N. Damil, "A dimensionless analytical analysis for buckling and lateral buckling interaction of thin-walled beams with open cross sections," *Thin-Walled Structures*, vol. 195, p. 111396, 2024, doi: 10.1016/j.tws.2023.111396.

[3] P. Rozylo, M. Rogala, and J. Pasnik, "Buckling Analysis of Thin-Walled Composite Structures with Rectangular Cross-Sections under Compressive Load," *Materials*, vol. 16, no. 21, p. 6835, 2023, doi: 10.3390/ma16216835.

[4] P. Różyło, K. Rosłaniec, and M. Kuciej, "Buckling of Compressed Thin-Walled Composite Structures with Closed Sections," *Advances in Science and Technology Research Journal*, vol. 17, no. 6, pp. 63-72, 2023, doi: 10.12913/22998624/174193.

[5] M. Grenda and P. Paczos, "Experimental and numerical study of local stability of non-standard thin-walled channel beams," *Journal of Theoretical and Applied Mechanics*, vol. 57, no. 3, pp. 549-562, 2019, doi: 10.15632/jtam-pl/109601.

[6] M. Grenda, "The Numerical Investigation of Thin-Walled Beams with Modified C-Sections," *Archives of Mechanical Technology and Materials*, vol. 38, no. 1, pp. 57-66, 2018, doi: 10.2478/amtm-2018-0010.

[7] P. Paczos and A. M. Pawlak, "Experimental optical testing and numerical verification by cufsm of compression columns with modified channel sections," *Materials*, vol. 14, no. 5, p. 1271, 2021, doi: 10.3390/ma14051271.

[8] P. Jasion, A. Pawlak, and P. Paczos, "Buckling and post-buckling behaviour of selected cold-formed C-beams with atypical flanges," *Engineering Structures*, vol. 244, p. 112693, 2021, doi: 10.1016/j.engstruct.2021.112693.

[9] M. Obst, M. Rodak, and P. Paczos, "Limit load of Cold formed thin-walled nonstandard channel beams," *Journal of Theoretical and Applied Mechanics*, vol. 54, no. 4, pp. 1369-1377, 2016, doi: 10.15632/jtam-pl.54.4.1369.

[10] E. Magnucka-Blandzi, P. Paczos, and P. Wasilewicz, "Buckling study of thin-walled channel beams with double-box flanges in pure bending," *Strain*, vol. 48, no. 4, pp. 317-325, 2012, doi: 10.1111/j.1475-1305.2011.00825.x.

[11] M. M. Yehia, S. M. Gaawan, R. Elwan, O. R. Shahin, and W. Z. El-sayad, "Structural performance evaluation of cold formed steel cantilever beams with varying perforation

Patterns," *Alexandria Engineering Journal*, vol. 91, pp. 204-221, 2024, doi: 10.1016/j.aej.2024.01.049.

[12] D. Dubina and V. Ungureanu, "Local/distortional and overall interactive buckling of thin-walled cold-formed steel columns with open cross-section," *Thin-Walled Structures*, vol. 182, p. 110172, 2023, doi: 10.1016/j.tws.2022.110172.

[13] X. Yao, J. Yang, and Y. Guo, "Study on Restoring Force Model of Cold-Formed Thin-Walled Steel Lipped Channel Beam-Columns under Cyclic Load," *Buildings*, vol. 13, no. 1, p. 114, 2023, doi: 10.3390/buildings13010114.

[14] M. Anbarasu, "A numerical investigation of local - distortional - lateral - torsional buckling interaction of cold - formed steel lipped channel beams," *Asian Journal of Civil Engineering*, vol. 18, no. 4, pp. 643-656, 2017.

[15] P. Borges Dinis and D. Camotim, "Local/distortional mode interaction in cold-formed steel lipped channel beams," *Thin-Walled Structures*, vol. 48, no. 10–11, pp. 771-785, 2010, doi: 10.1016/j.tws.2010.01.005.

[16] A. M. El Hadidy, M. F. Hassanein, and M. Zhou, "The effect of using tubular flanges in bridge girders with corrugated steel webs on their shear behaviour – A numerical study," *Thin-Walled Structures*, vol. 124, pp. 121-135, 2018, doi: 10.1016/j.tws.2017.11.050.

[17] M. Ghorashi, "Nonlinear static and stability analysis of composite beams by the variational asymptotic method," *International Journal of Engineering Science*, vol. 128, pp. 127-150, 2018, doi: 10.1016/j.ijengsci.2018.03.011.

[18] Md. Fayz-Al-Asad, F. Mebarek-Oudina, H. Vaidya, Md. Shamim Hasan, Md. Manirul Alam Sarker, and A. I. Ismail, "Finite Element Analysis for Magneto-Convection Heat Transfer Performance in Vertical Wavy Surface Enclosure: Fin Size Impact," *Frontiers in Heat and Mass Transfer*, vol. 22, no. 3, pp. 817–837, 2024.

[19] N. H. Abu-Hamdeh, K. Daqrouk, and F. Mebarek-Oudina, "Simulation and Analysis with Wavelet Transform Technique and the Vibration Characteristics for Early Revealing of Cracks in Structures," *Mathematical Problems in Engineering*, no. 2021, p. 626232, 2021, doi: 10.1155/2021/6626232.

[20] P. Manikandan and M. Thulasi, "Investigation on cold-formed steel lipped channel built-up I beam with intermediate web stiffener," *International Journal of Advanced Structural Engineering*, vol. 11, no. 1, pp. 97-107, 2019, doi: 10.1007/s40091-019-0220-x.

[21] P. Nandini and V. Kalyanaraman, "Strength of cold-formed lipped channel beams under interaction of local, distortional and lateral torsional buckling," *Thin-Walled Structures*, vol. 48, no. 10-11, pp. 872-877, 2010. doi: 10.1016/j.tws.2010.04.013.

[22] A. Gliszczyński and T. Kubiak, "Load-carrying capacity of thin-walled composite beams subjected to pure bending," *Thin-Walled Structures*, vol. 115, pp. 76-85, 2017, doi: 10.1016/j.tws.2017.02.009.

[23] J. Zhang and B. Young, "Finite element analysis and design od cold-formed steel built-up closed section columns with web stiffeners," *Thin-Walled Structures* , vol. 131, pp. 223-237, 2018, doi: 10.1016/j.tws.2018.06.008.

[24] K. Falkowicz and H. Debski, "Stability analysis of thin-walled composite plate in unsymmetrical configuration subjected to axial load," *Thin-Walled Structures*, vol. 158, p. 107203, 2021, doi: 10.1016/j.tws.2020.107203.

[25] H. Debski, "Numerical and experimental analysis of stability of thin-walled composite structures subjected to eccentric load," *Archives of Civil and Mechanical Engineering*, vol. 19, no. 3, pp. 792-802, 2019, doi: 10.1016/j.acme.2019.03.008.

[26] K. Magnucki, „Niektóre problemy optymalizacji konstrukcji prętowych i powłok z uwzględnieniem stateczności sprężystej," *Publishing House of Poznań University of Technology*, 1993.

[27] O. Hughes and M. Ma, "Lateral Distortional Buckling of Monosymmetric Beams under Point Load," *Journal of Engineering Mechanics*, vol. 122, no. 10, 1996, doi: 10.1061/(asce)0733-9399(1996)122:10(1022).

[28] F. Mohri, L. Azrar, and M. Potier-Ferry, "Flexural–torsional post-buckling analysis of thin-walled elements with open sections," *Thin-Walled Structures*, vol. 39, no. 11, pp. 907–938, 2001, doi: 10.1016/S0263-8231(01)00038-6.

[29] European Committee for Standardization [CEN], *prEN 1993–1–5, Eurocode 3: Design of steel structures – Part 1–5: Plated structural elements*, no. i. 2021.

[30] A. M. Pawlak, T. Górny, M. Plust, P. Paczos, and J. Kasprzak, "Imperfections in thin-walled steel profiles with modified cross-sectional shapes - Current state of knowledge and preliminary studies," *Steel and Composite Structures*, vol. 52, no. 3, pp. 327-341, 2024, doi: 10.12989/scs.2024.52.3.327.